

# Transient electrical conductivity of W-based electron beam induced deposits during growth, irradiation and exposure to air

F. Porrati, R. Sachser and M. Huth

*Physikalisches Institut, Goethe-Universität, Max-von-Laue-Str. 1, D-60438 Frankfurt am*

*Main, Germany*

## Abstract

W-based granular metals have been prepared by electron beam induced deposition from the tungsten-hexacarbonyl  $W(CO)_6$  precursor. *In situ* electrical conductivity measurements have been performed to monitor the growth process and to investigate the behavior of the deposit under electron beam post irradiation and by exposure to air. During the first part of the growth process, the electrical conductivity grows non-linearly, independent of the electron beam parameters. This behavior is interpreted as the result of the increase of the W-particles diameter. Once the growth process is terminated, the electrical conductivity decreases with the logarithm of time,  $\sigma \sim \ln(t)$ . Temperature-dependent conductivity measurements of the deposits reveal that the electrical transport takes place by means of electron tunneling either between W-metal grains or between grains and trap sites in the matrix. After venting the electron microscope the electrical

conductivity of the deposits shows a degradation behavior, which depends on the composition. Electron post-irradiation increases the electrical conductivity of the deposits.

## 1. Introduction

Electron beam induced deposition (EBID) is a high resolution one-step technique used to deposit and to pattern two- and three-dimensional micro- and nano-structures [1]. The importance of EBID is rapidly increasing in applied science and fundamental research [2]. On the one hand, the possibility of direct writing makes EBID a promising alternative to nano-lithography and a useful tool for mask repair. On the other hand, the capability to produce deposits from many different precursors with tunable electrical properties makes this technique attractive for the development of new materials. EBID is based on the interaction of an electron beam with a substrate which is covered by adsorbed precursor molecules and which contain the metal or semiconductor to be deposited. The electrons dissociate the precursor molecules into a volatile component, which leaves the surface and into a non-volatile one, which forms the deposit. The deposits consist of a disordered array of crystalline metallic nanoparticles with diameters between about 1 nm to 5 nm embedded in an insulating matrix. The metal volume fraction, i.e. the average particle size and the interparticle distance, can be varied by tuning the electron beam parameters (beam current, acceleration voltage, dwell time).

*In situ* electrical conductivity measurements of granular materials prepared by EBID or IBID (ion beam induced deposition) are valuable in order to study the growth process and the response of the material during post-irradiation and exposure to air. By

means of these measurements information about the electrical transport properties, the microstructure, the chemical and physical stability of the deposit are deduced. In literature, *in situ* electrical measurements of IBID and EBID deposits are rare [2]. The electrical behavior of EBID deposits from acrylic acid has been monitored by means of two-probe measurements [2]. Recently an ageing process has been monitored in platinum-based nanostructures [3]. The authors report a continuous decrease of the conductivity over a time range of many days. Studies performed by using  $W(CO)_6$  as a precursor are known for deposits produced by IBID [4] and EBID [5,6]. The investigation of Hoyle *et al.* [5,6] represents an important reference for the present study. In their work the authors prepared structures for beam energies between 2 keV and 20 keV. They investigated *in situ* the electrical conductivity of the deposits and, by means of transmission electron microscopy (TEM), their microstructure. It is the purpose of the present paper to further investigate the properties of W-based deposits from the  $W(CO)_6$  precursor by performing *in situ transient* electrical conductivity measurements during deposition, post-irradiation and exposure to air.

## 2. Experimental

To prepare our samples we used a dual beam SEM/FIB microscope (FEI, Nova Nanolab 600) with Schottky electron emitter and an ultimate resolution of 1 nm. In this system the electron beam power can be continuously tuned by means of the continuous variation of the beam energy and pre-defined discrete values of the beam current. The microscope is equipped with a gas injection module which introduces the  $W(CO)_6$  gas

precursor via a 0.5 mm diameter capillary in close proximity to the focus of the electron or ion beam on the substrate surface. EBID structures were grown on a Si (p-doped)/SiO<sub>2</sub> (300 nm) substrate. The substrates were pre-patterned with 120 nm thick Au/Cr contacts defined by UV-photolithography. In Fig. 1 we show a scanning electron microscope (SEM) image of three deposits for two-probe electrical measurements. This technique was chosen after having verified that the influence of the contact resistance between electrodes and deposits is below about 3%. Our chips are prepared to allow measurements for up to 12 deposits. After deposition in situ energy dispersive x-rays analysis (EDX) at 5 keV electron beam energy was performed in order to determine the material composition of the deposit. The low beam energy was chosen to avoid excitation of x-ray fluorescence in the substrate material. This was verified by Monte Carlo simulations of the electron trajectories for the given thicknesses and compositions of the deposit [7]. For in situ transient electrical conductivity measurements a Keithley Sourcemeter coupled with a Multiplexer was used to perform current measurements at fixed bias voltage. The conductivity was deduced from the known dimensions of the deposits. The lengths  $l$ , the widths  $w$  and the height  $h$  of the samples were determined by direct analysis of the SEM images. The maximum geometry-dependent error for the conductivity data amounts to about 35%. Finally, temperature-dependent measurements of the electrical conductivity were performed in a variable-temperature insert mounted in a <sup>4</sup>He cryostat in the temperature range 1.8-265 K.

### 3. Measurements

### 3.1 Deposition parameters and EDX characterization

In Fig. 2 we report the results of the composition analysis performed by means of EDX for the samples used in this work. The deposits have been obtained with a variable voltage and beam current in the range  $4 \text{ keV} \leq E \leq 20 \text{ keV}$  and  $0.25 \text{ nA} \leq I \leq 6.6 \text{ nA}$ , respectively. The corresponding beam power varied between  $5 \text{ nA} \cdot \text{keV} \leq p \leq 26 \text{ nA} \cdot \text{keV}$ . Within this range the deposits are granular with a W-content which increases linearly between 8.1 at% and 38.7 at%. In the left inset of Fig. 2 we plot the conductivity vs. the dose per scan. For high doses per scan the conductivity lies in the range between ca. 9300 to 18000  $\Omega^{-1}\text{m}^{-1}$ . These values are in agreement with the ones reported by Hoyle *et al.* [5, 6]. For smaller beam power we measure a strong decrease of the conductivity which reaches 17  $\Omega^{-1}\text{m}^{-1}$  at 65 C/m<sup>2</sup>. This value is one order of magnitude smaller than the one reported in Ref. [5, 6] for comparable dose per scan. On the right side of Fig. 2 we plot the ratio between oxygen (or carbon) and tungsten ( $[\text{O}]/[\text{W}]$  or  $[\text{C}]/[\text{W}]$ ) content vs. the tungsten-content for each deposit. The ratio  $([\text{O}]+[\text{C}])/[\text{W}]$  is also plotted. For W content equal to 8.1 at% we obtain  $([\text{O}]+[\text{C}])/[\text{C}]=11.4$ . This value is close to the one deducible from the stoichiometry of  $\text{W}(\text{CO})_6$  if one were to assume that the CO molecules do not dissociate. By increasing the beam power the W content increases, whereas the carbon and oxygen content decrease. Additional information can be deduced from the ratio  $[\text{C}]/[\text{O}]$  (see inset). For low doses we find  $[\text{C}]/[\text{O}]>1$ , which shows that the composition of the matrix is dominated by carbon. The  $[\text{C}]/[\text{O}]$  ratio shows a peak for a W content of ca. 15 at% and then it decreases towards 1. By means of TEM measurements

Hoyle *et al.* [5] found an amorphous material for deposits prepared with a dose per scan smaller than 500 C/m<sup>2</sup>. For higher doses they found W containing nanocrystals consistent with the high temperature  $\beta$ -phase of tungsten carbide ( $\beta$ -WC<sub>1-x</sub>). The nanocrystal size was estimated to be less than about 3 nm. From the EDX analysis of our deposits we point out that the [W] content increases with increasing beam power or with increasing dose per scan.

### 3.2 Measurements during growth

In Fig. 3 we show transient electrical conductivity measurements during the growth of deposits with a W content of 8.1 at% (sample #1), 14.7 at% (sample #4) and 38.7 at% (sample #9). For details concerning the composition, the geometry and the beam parameters used during deposition see Tab. 1.

At the time  $t = 10$  sec the gas precursor enters the vacuum chamber. The e-beam is rastered over a rectangular area defining the later deposit. In order to prepare samples #1 and #4 we used a dwell time of 100  $\mu$ s per pixel and a pitch of 20 nm. For sample #9 we used a dwell time of 5  $\mu$ s per pixel and a pitch of 20 nm. The conductivity changes at a rate  $\sigma' = \sigma/t$  which increases monotonically with time during the deposition of all samples. Sample #9 shows a rapid increase of  $\sigma'$  in the first seconds of deposition, which we attribute to the formation of the first layer of the deposit. In the first 5 seconds  $\sigma'$  follows a power law of the form  $\sigma' = t^\alpha$ , with  $\alpha = 3$ . After that,  $\sigma'$  drastically decreases tending to become constant, as can be expected, if the thickness of the deposit grows linearly with time.  $\sigma'$  for the deposits with 8.1 at% and 14.7 at% metal content follows a

Table 1: Composition and deposition parameters of the samples. Sample geometry ( $l/\mu\text{m} \times w/\mu\text{m} \times h/\text{nm}$ ), beam parameters (dwell time/ $\mu\text{s}$ , pitch/nm): Sample #1 ( $8.75 \times 1.03 \times 240$ ), (100, 20); #2 ( $9.19 \times 1.03 \times 315$ ), (100, 20); #3 ( $8.27 \times 1.06 \times 226$ ), (100, 20); #4 ( $4.76 \times 1.09 \times 228$ ), (100, 20); #5 ( $6.15 \times 1.03 \times 148$ ), (100, 20); #6 ( $18.1 \times 1 \times 352$ ), (100, 20); #7 ( $4.57 \times 1.03 \times 241$ ), (100, 20); #8 ( $14.93 \times 1.63 \times 192$ ), (100, 20); #9 ( $7.75 \times 1.51 \times 682$ ), (5, 20).

Sample	W [at%]	C [at%]	O [at%]	Energy/keV	Current/nA
#1	8.1	66.4	25.5	20	0.25
#2	8.9	69.8	21.3	24	0.28
#3	9.0	64.9	26.1	20	0.25
#4	14.7	67.5	17.9	20	0.5
#5	15.6	68.9	15.6	20	0.51
#6	16.7	66.7	16.6	11	2.3
#7	31.5	21.1	47.4	17	1.52
#8	31.8	44.4	23.8	5	3.7
#9	38.7	34.7	26.6	4	6.6

power law of the form  $\sigma' \sim t^\alpha$ , with  $\alpha = 1.86$  and  $\alpha = 1.43$ , respectively. For sample #1  $\sigma'$  follows this power law during the whole deposition process, for the sample #4 it shows a decrease after about  $t = 10^3$  s. The fit to sample #4 was made between 300 and 1000 seconds. In this range the growth rate is lower than in the first 300 seconds of deposition,

which we excluded from the fit because of the high dispersion of the experimental points. Therefore it is not surprising that the result of the fit gives for  $\alpha$  a value larger for sample #1 than for sample #4, which is counterintuitive since we expect higher growth rate for deposits with higher metal content.

In conclusion, these results clearly indicate that a linear increase of the thickness is not sufficient to explain the transient electrical conductivity measurements during the growth of the deposits. Since the increase of the conductivity is faster than linear, an additional mechanism has to be considered in order to understand this observation. Among the possible mechanisms which may contribute to the enhancement of  $\sigma'$  we consider the charging effect and the increase of the metal grain size due to the electron beam irradiation. In the last chapter of the paper we discuss the relevance of these mechanisms for the samples prepared in this work.

The growth process terminates with the simultaneous shut-off of the electron beam and the precursor gas supply. Correspondingly, the conductivity starts to decrease (see Fig. 3). The relaxation of the conductivity can be attributed to the migration of excess electrons injected by the electron beam towards the electrodes. In Fig. 4a we depict the relaxation for samples #1, #4 and #9. The conductivity relaxation follows a logarithmic time dependence, i.e.,  $\sigma = b \cdot \ln(t)$ . With suitable choice of the parameter  $b$ , this formula can be used to fit the relaxation of all the deposits. The velocity of the relaxation depends on the deposits' composition. In particular, we notice that deposits with lower W content relax more rapidly than deposits with higher W content. This information is



summed up in Fig. 4b for all the samples prepared in this work.

### 3.3 Measurements during venting the microscope

Transient electrical conductivity measurements during exposure to air were performed after deposition by venting the electron microscope. The result of these experiments are summarized in Fig. 5 where we plot the normalized conductivity vs. time for various deposits. The venting procedure starts at  $t=60$  s, when  $N_2$  gas enters the chamber. The conductivity of the deposits starts to decrease with a rate which depends on the metal concentration. In particular, the lower is the metal content the faster is the decrease. The reduction of the conductivity becomes faster at  $t\approx 400$  s, when the door of the chamber slightly opens and a small flux of air enters the microscope. At  $t\approx 900$  s the door of the microscope is deliberately opened to fully expose the deposits to air. At this point the reduction rate of the conductivity strongly increases. According to Fig. 5, we divide the deposits in two groups exhibiting strong and weak degradation of the conductivity, respectively. To the first group belong the samples #1, #2, #5 with metal content equal to 8.1 at%, 8.9 at% and 15.6 at%. After one hour from opening of the vacuum chamber the conductivity of these deposits has dropped to 7 % to 34 % of its initial value. To the second group belong samples #6, #7, #9 with 16.7 at%, 31.5 at% and 38.7 at%. In this case after one hour of exposure the value of the conductivity lies between 90 % and 99 % of the initial value. It is interesting to note that the degradation rate increases monotonically with decreasing metal content and, thus, with the beam power used to prepare the respective samples. Most likely the degradation is due to a reduction of the

tunneling probability within the deposit. In the discussion section we speculate that the degradation rate can be linked to the density of the deposit which depends on the beam power [8].

### 3.4 Post-irradiation conductivity behavior

In order to study the effect of the beam irradiation on EBID deposits we consider two samples with W content of 9 *at%* (sample #3) and 14.7 *at%* (sample #4), respectively. After preparation the samples were irradiated with the same beam power used during deposition, i.e. 5 nA·keV and 10 nA·keV, respectively. In Fig. 6a we plot the transient conductivity vs. the irradiation time. The conductivity of both samples abruptly increases during the first few seconds of irradiation. In the following minutes the conductivity increases monotonically at a much lower rate, which depends on the composition of the deposit. The conductivity of sample #3 increases to approximately eight times its initial value in 2000 seconds of irradiation. In the same time interval the conductivity of sample #4 increase only by 10 % of its initial value. The increase of conductivity may be attributed to the increase of charge carriers released during the beam-induced breakage of carbon-carbon bonds in the amorphous matrix, as was speculated in Ref. [9, 10]. Sample #3 shows the largest increase of conductivity because it is the sample with largest matrix volume fraction. In Fig. 6b we report the relaxation of the conductivity over a time scale of almost 3 days. The most remarkable fact is the very low decrease of the conductivity in comparison with its increase during post-irradiation. The second remarkable fact is that the conductivity is not logarithmically dependent on time. Therefore no relax-

ation of the conductivity takes place; rather, we suggest that the conductivity deteriorates because of the exposure to the rest gases present in the SEM chamber. The phenomena is similar to the one occurring by exposure to air. However, its time scale is much longer because the residual pressure ( $\approx 4 \cdot 10^{-6}$  mbar) inside the microscope is order of magnitude lower than in the environment. Note that in the frame of the "bond-breaking"-model we expect that carbon atoms bond again leading to a conductivity decrease much faster than the one observed. Therefore we attribute the increasing conductivity during irradiation to a permanent chemical transformation of the deposit.

### 3.5 Temperature dependence of the electrical conductivity

In this section we present the temperature-dependent conductivity measurements performed for the samples with W content of 8.1 at% (sample #1), 14.7 at% (sample #4) and 31.8 at% (sample #8). For the low conductivity samples #1 and #4 we choose an applied field between 1143 V/cm and 210 V/cm in order to be able to measure  $\sigma(T)$  down to the lowest temperature accessible in our setup. In order to avoid irreversible switching in the  $I(V)$  characteristic during the measurements we used a current limit. For sample #8 we choose an applied field of 6.7 V/cm in order to measure  $\sigma(T)$  in the linear regime of the  $I(V)$  characteristic. In Fig. 7a we plot the conductivity vs. temperature dependence for samples #1 and #4. Both samples show the characteristic of systems governed by variable-range-hopping, i.e.  $\sigma = \sigma_0 \exp(T_0/T)^\alpha$ . In particular, we observed  $\alpha = 0.28$  and  $\alpha = 0.37$  for samples #1 and #4, respectively. The behavior in the system with lowest metal content is close to that one of amorphous carbon films [11, 12]. In that

case the tunneling takes place between localized sites in the limit of negligible Coulomb blockade effects ( $\alpha = 0.25$ ) [11]. The value of  $\alpha$  obtained for sample #4 may suggest both, a contribution to the tunneling between the trap sites in the matrix and between the metal grains; the latter mechanism is described by the exponent  $\alpha = 0.5$  [13, 14]. In Fig. 7b we plot the temperature dependence of the electrical conductivity for sample #8. We find that the conductivity follows a power law over the complete temperature range of our measurement ( $1.8 \text{ K} \leq T \leq 265 \text{ K}$ ) with  $\sigma = \sigma_0 + a T^\beta$ , with  $\beta = 0.55$ . Such a behavior is similar to the one recently reported in Ref. [15] and interpreted by means of a tunneling percolation model in the limit of large inter-grain tunneling [15, 16].

#### 4. Discussion

A linear increase of the time-dependent conductivity can be explained by supposing a linear time dependent growth of the thickness. However, the measurements performed during growth show an increase of the conductivity vs. time faster than linear. Therefore, an additional mechanism which contributes to the enhancement of the conductivity has to be considered. Possible additional mechanisms for the increase of the conductivity growth-rate include an enhancement of the electron carrier density and of the metal-particles' size during deposition, both due to the electron beam irradiation. In the following we relate the time dependence of the conductivity to the increase of the metal particles' size by means of a "shell-model". We consider a sphere of radius  $r$  and volume  $v_s$  representing a metal-particle, see Fig. 8. Coordination sphere of radius  $l$  and volume  $v_l$  surrounds the first one. The radius difference  $s=l-r$  represents the separation between two neighboring

particles. The ratio  $v = v_s/v_l$  gives the metal-volume fraction of the system. It follows that the diameter of the metal particle is  $d = 2 r = 2 l v^{\frac{1}{3}}$ . We suppose that at time  $t=t_0$  the deposit is constituted by particles with the same radius  $r$ . The particles of this initial deposit increase their volume because of electron beam stimulated diffusion of W-atoms. In general, the growth rate of the particle size is described by the Lifshitz-Slyozov coarsening law  $r \sim t^{\frac{1}{3}}$  [17]. However, also lower growth rates with  $r \sim t^{\frac{1}{n}}$  with  $n>3$ , have been reported [18,19], which indicate diffusion limited mass transport. Known the diameter  $d$ , the separation  $s$  and the growth rate, the time-dependence conductivity in the VRH regime can be deduced from equation (1)

$$\sigma \sim e^{-2\frac{s}{\xi} - \frac{W}{k_B T}} \quad (1)$$

where  $\xi$  is the localization length,  $k_B$  the Boltzmann constant,  $T$  the temperature and  $W$  the effective activation energy for charge transport [20,21]. The time dependence of the conductivity is implicit in the localization length and in the activation energy, both dependent on the particle diameter. In particular,  $\xi = \xi_{mx}(1 + d/s)$ , with  $\xi_{mx}$  being the localization length of the matrix [20]. The localization length is obtained from the relation  $\xi_{mx} = 2.8e^2/4\pi\epsilon\epsilon_0k_B T_0(1 + d/s)$  [22], where  $\epsilon$  is the dielectric constant of the deposit and  $T_0$  a constant deducible from the temperature-dependent conductivity measurements. From the experiments one also extracts the activation energy  $W=\alpha kT(T_0/T)^\alpha$  [20]. From Fig 7a it results  $T_0 = 1.28 \cdot 10^5$  K and  $T_0 = 6.4 \cdot 10^3$  K, for samples #1 and #4, respectively. The values of the dielectric constant necessary to calculate  $\xi_{mx}$  are chosen considering that

for a carbon-matrix  $\epsilon \approx 4$  [23] and that with increasing metal volume fraction, the dielectric constant of a metal-insulator composite increases [24]. By using for  $\epsilon$  the values 8 and 12, it follows  $\xi_{mx} = 0.02$  nm and  $\xi_{mx} = 0.1$  nm,  $\xi = 0.03$  nm and  $\xi = 0.61$  nm for samples #1 and #4, respectively. For a comparison note that the value of the localization length of amorphous carbon thin films lies between 0.1 nm and 1.2 nm [25]. In Fig. 9 we report the time-dependent conductivity measurements for samples #1 and #4. In order to fit the experimental data, we choose a linear increase of the metal volume fraction  $v$  from 0.04 to 0.06 and from 0.04 to 0.35 for samples #1 and #4, respectively. The best fit was obtained with  $n=9.8$  and  $n=6.3$ ,  $0.61 \leq s/l \leq 0.65$  and  $0.28 \leq s/l \leq 0.66$ , respectively for samples #1 and #4. These choices for  $l$  and  $v$  lead to  $0.55 \text{ nm} \leq s \leq 0.59 \text{ nm}$  and  $0.42 \text{ nm} \leq s \leq 0.99 \text{ nm}$ ,  $0.62 \text{ nm} \leq d \leq 0.71 \text{ nm}$  and  $1.03 \text{ nm} \leq d \leq 2.16 \text{ nm}$ , respectively for the two samples. In conclusion, the experimental data on the growth process can be well described within our "shell-model" by using a coarsening growth rate which depends on the deposit's metal content and, thus, on the beam parameters. We find that in the deposit with lowest metal content (sample #1,  $n=9.8$ ) the size of the metal particle increases in time with the lowest rate, as one may have expected. The coarsening law of Lifschitz-Slyozov is not reached by the range of beam parameters used for sample #1 and #4. We believe that for higher deposition rates, such regime may be reached. It has to be noted that we cannot describe the behavior of sample #9 by means of the previous modelling because the parameters  $T_0$  and  $\xi$  cannot be deduced from the temperature dependence of the conductivity of Fig. 7b. However, it is quite possible that

in the first stages of the deposition process the electron transport may be described by the VRH mechanism. In this case, the growth rate of the particle size of sample #9 shall be much higher than the one of samples #1 and #4, being close to the Lifschitz-Slyozov theory. Indeed, an hint that this may be the case is given by the different power law, which is  $\sigma = t^4$  for sample #9 in the first seconds of deposition, while it is  $\sigma = t^{2.86}$  for sample #1, during the whole range of deposition time. It is important to note that the "shell-model" assumes the presence of nanocrystal particles in the deposit. According to the TEM measurements of Hoyle *et al.* [5] this assumption is fully justified for deposits prepared with high doses. For deposits prepared with a dose per scan smaller than 500 C/m<sup>2</sup> the authors of Ref. [5] found amorphous material. However, the presence of very small crystals not detectable from TEM measurements cannot be excluded. Indeed, the sharp fall of the conductivity with the decrease of the doses (see inset in Fig. 2) may also be explained by the Coulomb blockade of small nanocrystals at room temperature.

In granular materials it is observed that in the low conductivity tunneling regime the temperature dependence of the electrical conductivity is of the form  $\sigma \sim \exp(T_0/T)^\alpha$ , with  $0.25 \leq \alpha \leq 0.5$ . For our samples we find  $0.36 \leq \alpha \leq 0.5$  with metal content  $\leq 19\%$ , which may indicate a tunneling mechanism either involving localized sites in the matrix or directly between the metal grains. However, in order to have tunneling the typical hopping distance for the electron,  $r^* = (\frac{e^2\xi}{4\pi\epsilon\epsilon_0 k_B T})^{0.5}$ , has to be larger than the distance  $s$  between the localized states [22]. For the samples #1 and #4 we obtain  $r^*=0.46$  nm and  $r^*=1.69$  nm, respectively. By comparing these numbers with the ones for  $s$  given above

by the "shell-model" we find that in our deposits direct tunneling between grains appears to be possible. On the other hand, tunneling between localized sites in the matrix is not favorable. However, this does not exclude conduction inside the matrix which may also take place between localized matrix sites bridged by metal grains. As a consequence in the following we speculate that the transport mechanism in our deposits takes place by means of two channels: directly between grains and indirectly between localized sites in the matrix through a grain. In order to describe the transport mechanism we use the following formula:

$$\sigma = a \cdot \sigma_{01} \cdot e^{-\left(\frac{T_{01}}{T}\right)^{\frac{1}{4}}} + b \cdot \sigma_{02} \cdot e^{-\left(\frac{T_{02}}{T}\right)^{\frac{1}{2}}} + \sigma_{03} \cdot e^{-\left(\frac{T_{03}}{T}\right)^{\delta}} \quad (2)$$

The first two terms of equation (2) take into account the tunneling of electrons between trap sites in the matrix and between grains, respectively. The factor  $a$  gives the volume concentration of the matrix, while  $b$  refers to the concentration of the metal. The third term of the equation takes into account the hopping of electrons between trap sites and grains. The temperature  $T_{03}$  and factor  $\delta$  are free parameters. By fitting the experimental curves with equation (2), we obtain the volume concentration of the matrix and of the metal. We made the fit to the two curves of Fig. 7 ("fit 1" and "fit 2"), for which we have W content of 8.1at% and 14.7at%, associated to  $\alpha = 0.39$  and  $\alpha = 0.36$ , respectively. For the fit we set  $\sigma_{01} = 10 \Omega^{-1} \text{ cm}^{-1}$ ,  $T_{01} = 10^7 \text{ K}$  [25],  $\sigma_{02} = 27 \Omega^{-1} \text{ cm}^{-1}$  and  $T_{02} = 2070 \text{ K}$  [15]. For the third term of eq. (2) we choose  $\sigma_{03} = 15 \Omega^{-1} \text{ cm}^{-1}$ ,  $T_{03} = 1.3 \cdot 10^4 \text{ K}$  (fit 1) and  $T_{03} = 7 \cdot 10^3 \text{ K}$  (fit 2). The best fit was obtained for  $a = 0.06$ ,  $b = 0.94$  and



$\delta = 0.38$  (fit 1) and  $a = 0.35$ ,  $b = 0.65$  and  $\delta = 0.38$  (fit 2). We can compare the fractional volume obtained by the fit with the one deduced by EDX measurements. The fractional volume occupied by the metal particles depends on the density of the metal and of the matrix, which is not well known. The lower and upper limit corresponding to a density of  $1.8 \text{ g/cm}^3$  (graphite-like amorphous) and of  $3.5 \text{ g/cm}^3$  (diamond-like) lead for the W-content of 8.1at% to a fractional volume between 12vol% and 20vol% [15]. From our fit we obtain the volume of 6%, which would indicate a lower density than a graphite-like matrix. This difference may be due to the presence of oxygen atoms inside the carbonaceous matrix. By means of in situ mass measurements the density of the matrix of a W-based deposits from  $\text{W}(\text{CO})_6$  has been related to the electron beam parameters used during deposition [8]. In general, the density of the matrix increases with the power of the electron beam. The authors measured a matrix density between  $0.29 \text{ g/cm}^3$  and  $0.88 \text{ g/cm}^3$  corresponding to a W-volume concentration between 11.1 vol% and 6.4 vol% [8, 26]. These results were obtained for beam voltages between 5 keV and 15 keV, but with a beam current much higher than the one used in our depositions. For a system with W-content of 14.7at%, we calculate a fractional volume between 19vol% and 33vol% for graphite- and diamond-like matrix, respectively. The value of 35 vol% obtained within our modelling is close to that for a diamond-like matrix. Of course the matrix of our deposit is non-crystalline and does also contain oxygen. In conclusion, we find clear evidence of an increase of the density of the matrix by increasing the electron beam power. This result is in accord with the one obtained for amorphous carbon deposits

obtained by electron-beam-induced deposition [8, 26].

After terminating the growth process the conductivity starts to decrease with the logarithm of the time, see Fig. 4. The relaxation can be attributed to the migration of the charge carriers out of the sample. In general, in order to describe the relaxation of a system toward equilibrium a stretched exponential of the form  $\sigma \sim \exp(-t/\tau)^\beta$ , with  $0 \leq \beta \leq 1$  can be used [27]. In the case of  $\beta=1$  the Debye relaxation is obtained, which is valid for systems with weak dynamic correlations. In the case of hopping conductivity, this corresponds to a system with no Coulomb interactions. If the system presents strong dynamic interactions, the law of Kohlrausch [27] can be obtained by considering a serial relaxation of hierarchies of correlated systems [28]. In case of hopping conductivity, this corresponds to a system with strong Coulomb interactions, dynamically described by the tunneling of an electron into a localized state, which is possible if a second electron tunnels into another localized state (co-tunneling). The logarithmic decay of the variable describing a system finds an explanation in the frame of hierarchically constrained dynamics [29]. In particular, in the theoretical study of Ref. [30] it is mentioned that the conductivity of systems governed by hopping conduction can exhibit a logarithmic time dependence, as we find experimentally. Finally, we observed an increase of the relaxation rate at lower W-concentration. We attribute this behavior to the increased number of localized sites in the matrix and, therefore, to an higher probability for the electron to tunnel into a free localized state.

The increase of the density of the matrix with the electron beam current (see above)

can be used to interpret the conductivity measurements obtained during air exposure. The degradation rate  $\sigma'$  decreases as one considers deposits prepared at larger beam current (power) and, thus, with the density of the matrix. In order to better describe the degradation process, we fit the experimental data of Fig. 5, from the time where the door of the microscope is opened ( $t \approx 900$  s), with a sum of two exponential functions:  $\sigma \propto a_1 \exp(t/\tau_1) + a_2 \exp(t/\tau_2)$ . In Fig. 10a we plot a typical decay fitted with such a curve. In Fig. 10b we report the decay constants  $\tau_1$  and  $\tau_2$  for the deposit measurements depicted in Fig. 5 as a function of the beam power used to prepare the samples. Both decay constants increase with the beam power with  $(15 \leq \tau_1 \leq 236) \text{ s}^{-1}$  and  $(510 \leq \tau_2 \leq 2185) \text{ s}^{-1}$ . As one observes from the inset of Fig. 10b the weight of the first term of the exponential sum is larger than the weight of the second one ( $a_1 > a_2$ ). In particular the ratio strongly increases for small values of the beam power, which corresponds to deposits mainly constituted by the matrix. Therefore we associate the first term of the exponential sum to the matrix. The decay constant  $\tau_1$  is associated to the decrease of the tunneling probability within the matrix, or between matrix and grains in view of our previous discussion. The increase of the decay constant  $\tau_1$  with beam power is interpreted as due to the increase of the matrix density. The second term of the exponential sum may describe the decay of the tunneling probability between metal grains. The increase of the decay constant  $\tau_2$  with beam power may be interpreted as due to the increase of the grain size.

Similar considerations are useful in order to analyze the behavior of the deposits after irradiation. Also in this case the conductivity can be described by the sum of two

exponential functions. The two decays are independent processes linked to the decrease of the tunneling probability within the matrix and between the metal grains. The decay constants of sample #4 and sample #3 are  $\tau_1=1.91\cdot 10^4$  s,  $\tau_1=2.33\cdot 10^4$  s and  $\tau_2=1.66\cdot 10^5$  s,  $\tau_2=1.6\cdot 10^5$  s, respectively. These values are 2 to 3 orders of magnitude larger than those obtained by venting the system. From the literature it is known that the presence of residual oxygen and water molecules inside a SEM is sufficient to oxidize W-based granular metals prepared from the tungsten hexafluoride ( $WF_6$ ) precursor [31]. Similarly, the oxidation of the deposits is most likely the reason for the observed decrease of the conductivity that we measured inside the SEM. As can be expected, the degradation takes place on a much longer time scale in comparison to the exposure to air.

## 5. Conclusions

Probably, the most relevant technological aspect concerning our study is the investigation of the behavior of W-based granular metals during exposure to air. We have found that the degradation of the system strongly depends on the composition. In particular, after one hour of exposure to air the remaining conductivity varies between 7% and 99% of its initial value for deposits with W-content in the range  $8.1\text{at}\% \leq W \leq 38.7\text{at}\%$ . Transient electrical conductivity measurements indicate that this dependence is due to the different densities of the deposits. Furthermore, the decay of the conductivity involves the matrix and the W-metal grains on two different time scales. In conclusion, in view of the possible employment of EBID W-based deposits for applications the composition of the composite has to be carefully chosen to minimize ageing effect. In this direction it is

remarkable that after one year from deposition two samples with W-content of 34% and 19%, respectively, show a decrease of the conductivity only of a factor between two and four. However, covering the deposit with a protective  $\text{SiO}_x$ , layer like tetraethylorthosilicate (TEOS) precursor, may be necessary to prevent long time scale degradation of the electrical properties [3].

By means of transient electrical conductivity measurements we have monitored the growth process of W-based deposits. In order to explain the non-linear growth of the conductivity vs. time we have used a "shell-model" based on the hypothesis that the diameter of the W-metal particles grows during deposition. Within the modelling we have estimated the average particle size in the final deposit, which ranges between 0.71 nm and 2.16 nm for deposits with W content of 8.1at% and 14.7at%. It would be interesting to integrate this analysis with transmission electron microscopy investigations.

Furthermore, we have investigated the electrical transport mechanism as a function of the deposits' composition by means of conductivity vs. temperature measurements. From the analysis of the experimental data we have speculated that the electrical transport takes place by means of two parallel channels involving both the direct tunneling between metal-particles and the indirect tunneling between localized sites in the matrix bridged by metal particles. As a consequence of this investigation information about the matrix density can be deduced, which is useful to interpret the data of the conductivity degradation under exposure to air. Finally, we have observed that the relaxation of the charge carriers after termination of the deposition process follows a logarithmic time dependence. Such

a behavior suggest that at the end of the deposition the electron transport in the deposits is dominated by strong Coulomb interaction and that the relaxation can be described in the framework of hierarchically constrained dynamics commonly used to describe strongly interacting glassy materials.

In conclusion, we have shown that by means of *in situ* transient electrical conductivity measurements very useful information about the electrical transport mechanism, the microstructure and the chemical and physical stability of W-based granular materials can be obtained. It shall be interesting to extend this measurements to materials grown with other precursor gases and to further these studies with TEM investigations.

## **Acknowledgments**

Financial support by the *NanoNetzwerkHessen (NNH)* and by the *Bundesministerium für Bildung und Forschung (BMBF)* under grant 0312031C is gratefully acknowledged.

## References

- [1] Koops H W P, Kretz J, Rudolph M and Weber M 1993 *J. Vac. Sci. Technol. B* **11** 2386
- [2] Utke I, Hoffmann P and Melngailis J 2008 *J. Vac. Sci. Technol. B* **26** 1197
- [3] Botman A, Hesselberth M and Mulders J J L 2008 *J. Vac. Sci. Technol. B* **26** 2464
- [4] Prestigiacomo M, Roussel L, Houël A, Sudraud P, Bedu F, Tonneau D, Safarov V and Dallaporta H *et al.* 2004 *Microelectron. Eng.* **76** 175
- [5] Hoyle P C, Cleaver J R A and Ahmed H 1996 *J. Vac. Sci. Technol. B* **14** 662
- [6] Hoyle P C, Ogasawara M, Cleaver J R A and Ahmed H 1993 *Appl. Phys. Lett.* **62** 3043
- [7] Casino (Monte Carlo simulation of electron trajectories in solids) v2.42
- [8] Sawaya S, Akita S and Nakayama Y 2006 *Appl. Phys. Lett.* **89** 193115
- [9] Bret T 2005 *PhD Thesis* EPFL Lausanne
- [10] Babcock L E and Christy R W 1972 *J. Appl. Phys.* **43** 1423
- [11] Ambegaokar V, Halperin B I and Langer J S 1971 *Phys. Rev. B* **4** 2612-2620
- [12] Hauser J J 1977 *J. Non-Cryst. Solids* **23** 21-41
- [13] Abeles B, Sheng P, Coutts M D and Arie Y 1975 *Adv. Phys.* **24** 407
- [14] Sheng P, Abeles B and Arie Y 1973 *Phys. Rev. Lett.* **31** 44
- [15] Huth M, Klingenberg D, Grimm Ch, Porrati F and Sachser R 2008 *New J. Phys.*, submitted
- [16] Beloborodov I S, Efetov K B, Lopatin A V and Vinokur V M 2003 *Phys. Rev. Lett.* **91** 246801
- [17] Lifshitz I M, Slyozov V V 1961 *J. Phys. Chem. Solids* **19** 35

- [18] Goldfarb I, Hayden P T, Owen J H G and Briggs G A D 1997 *Phys. Rev. B* **56** 10459
- [19] Muratov C B 1998 *Phys. Rev. Lett.* **81** 3699
- [20] Adkins C J 1989 *J. Phys.: Condens. Matter* **1** 1253
- [21] Entin-Wohlman O, Gefen Y and Shapira Y 1983 *J. Phys. C* **16** 1161
- [22] Tran T B, Beloborodov I S, Lin X M, Bigioni T P, Vinokur V M and Jaeger H M 2005 *Phys. Rev. Lett.* **95** 076806
- [23] Grill A 2001 *Diamond Relat. Mater.* **10** 234
- [24] Efros A L and Shklovskii B I 1976 *Phys. Status Solidi B* **76** 475
- [25] Frauenheim Th, Stephan U, Bewilogua K, Jungnickel F, Blaudeck P and Fromm E 1989 *Thin Solid Films* **182** 63
- [26] Nishio M, Sawaya S, Akita S and Nakayama Y 2005 *J. Vac. Sci. Technol. B* **26** 1975
- [27] Kohlrausch R 1847 *Ann. Phys. (Leipzig)* **72** 394
- [28] Palmer R G, Stein D L, Abrahams E and Anderson P W 1984 *Phys. Rev. Lett.* **53** 958
- [29] Brea J J and Prados A 2001 *Phys. Rev. B* **63** 021108
- [30] Tsigankov D N, Pazy E, Laikhtman B D and Efros A L 2003 *Phys. Rev. B* **68** 184205
- [31] Klein K L, Randolph S J, Fowlkes J D, Allard L F, Meyer III H M, Simpson M L and Rack P D 2008 *Nanotechnology* **19** 345705



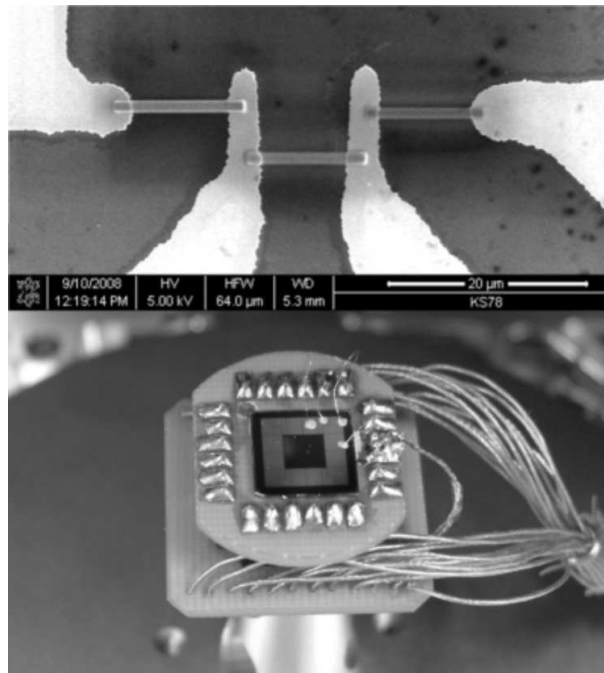


Figure 1: Upper figure: SEM image of three EBID structures for two-probe electrical measurements. The deposits are written on 120 nm thick gold/chromium electrodes. Lower figure: Setup for the *in situ* transient electrical conductivity measurements. On this chip 3 from 12 possible measuring positions are contacted via this copper wires attached to the contact pads with silver paint.

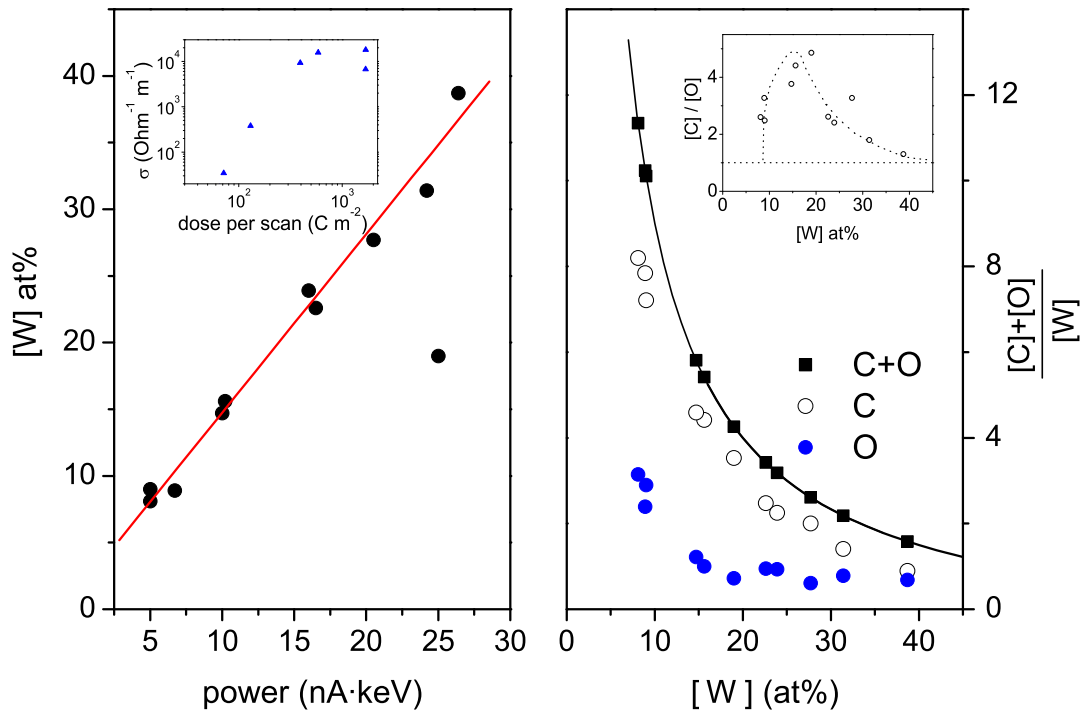


Figure 2: Left figure: Dependence of the W-metal content on the electron beam power. The conductivity increases with the dose used during deposition, see inset. Right figure: EDX analysis of the composition of the samples prepared in this work. The concentration of carbon and oxygen decrease with increasing power of the electron beam. In the inset we report the ratio between carbon and oxygen.

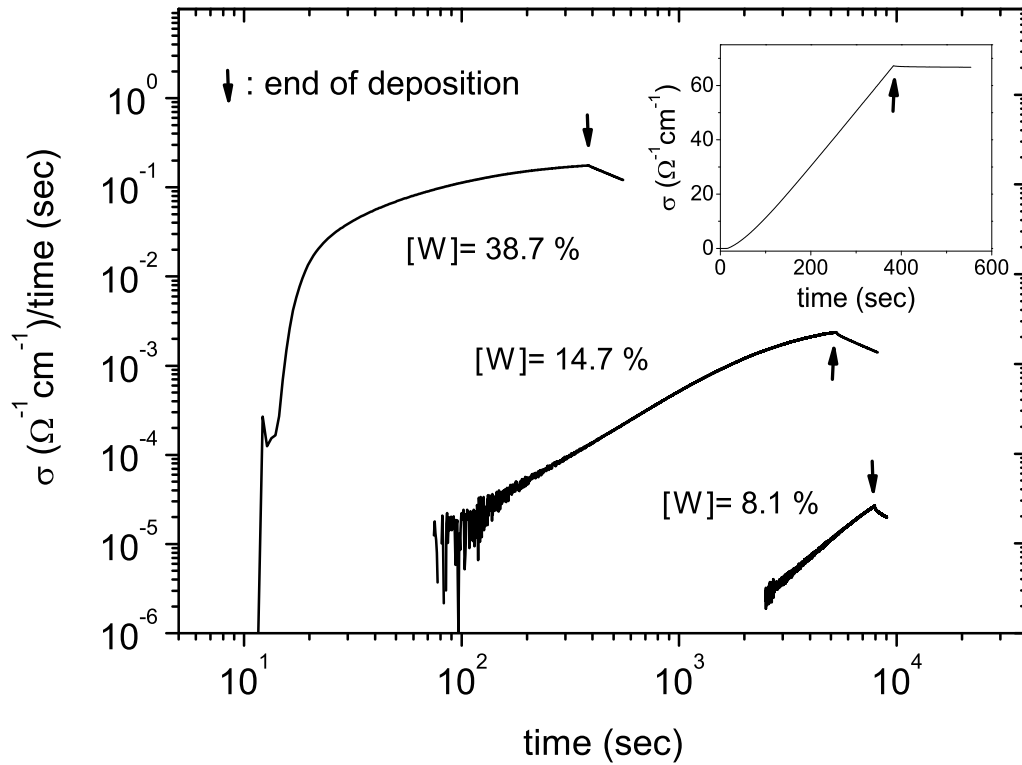


Figure 3: Electrical conductivity measured during the growth of sample #1 (8.1 at% W), #4 (14.7 at%) and #9 (38.7 at%), respectively. In each case, the deposition was started at  $t=10$  sec. The data points in the inset for sample #9 show that after an initial non-linear growth, the conductivity tends to increase linearly with the time. The conductivity of samples #1 and #4 is non-linear during the whole deposition time considered, which is due to the lower growth rate of these deposits. The electrical conductivity of each sample decreases once the deposition process is terminated.

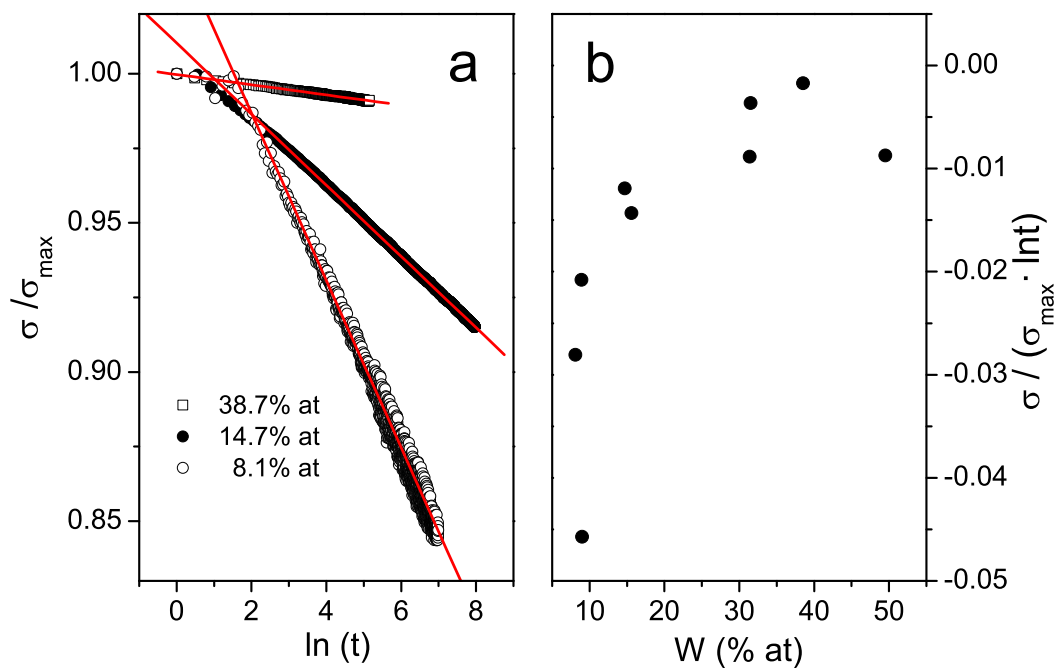


Figure 4: a: Relaxation of the conductivity after the end of the deposition process. The conductivity decreases with the logarithm of the time,  $\sigma = b \cdot \ln(t)$ . b: Relaxation rate vs. metal content. The lower the metal content the faster the relaxation rate.

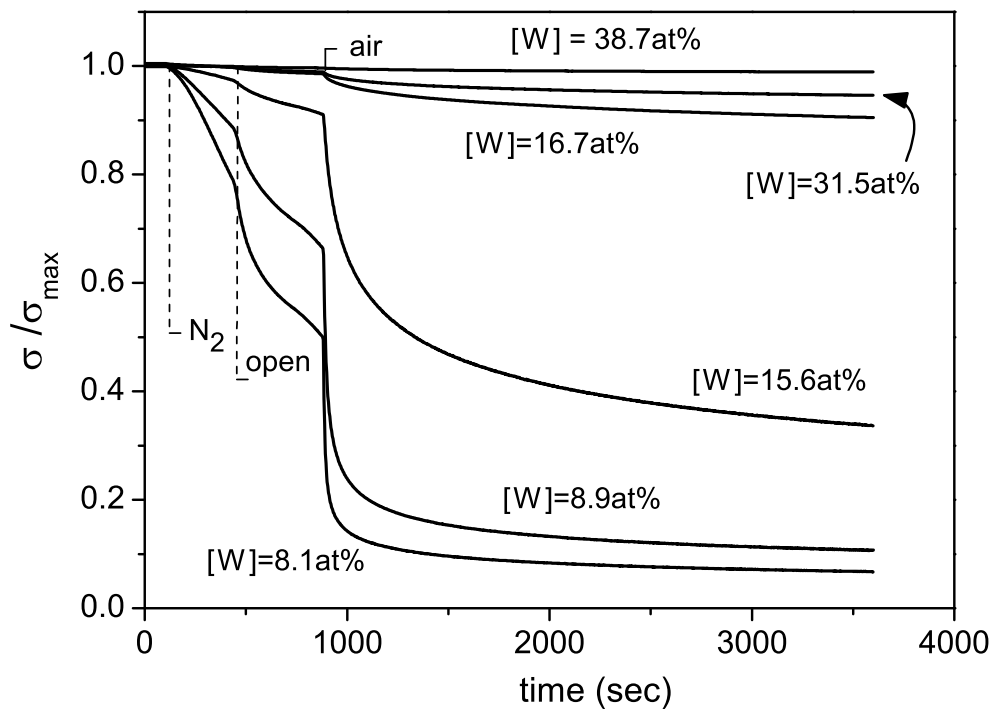


Figure 5: Electrical conductivity vs. time as the SEM is vented. During the procedure first nitrogen enters the chamber; after ca. 6 minutes the door of the microscope slightly opens. 8 minutes later the door is fully open. The conductivity decreases with time at a rate which depends on the material composition. See text for details.

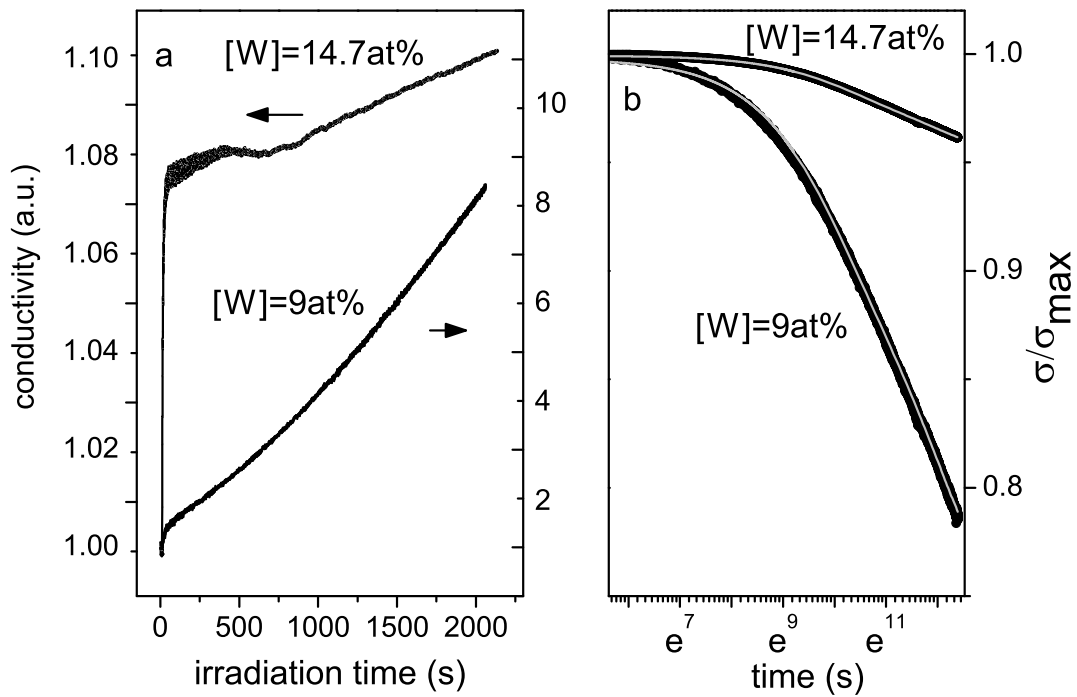


Figure 6: Post-irradiation experiment. Left figure: Conductivity vs. irradiation time. The increase of the conductivity is the highest for the sample with lowest W content. Right figure: evolution of the conductivity after termination of the irradiation. The decay of the conductivity is described by two parallel decay channels involving the matrix and the W grains. The fastest decay is for the deposit with the lowest W content. See text for details.

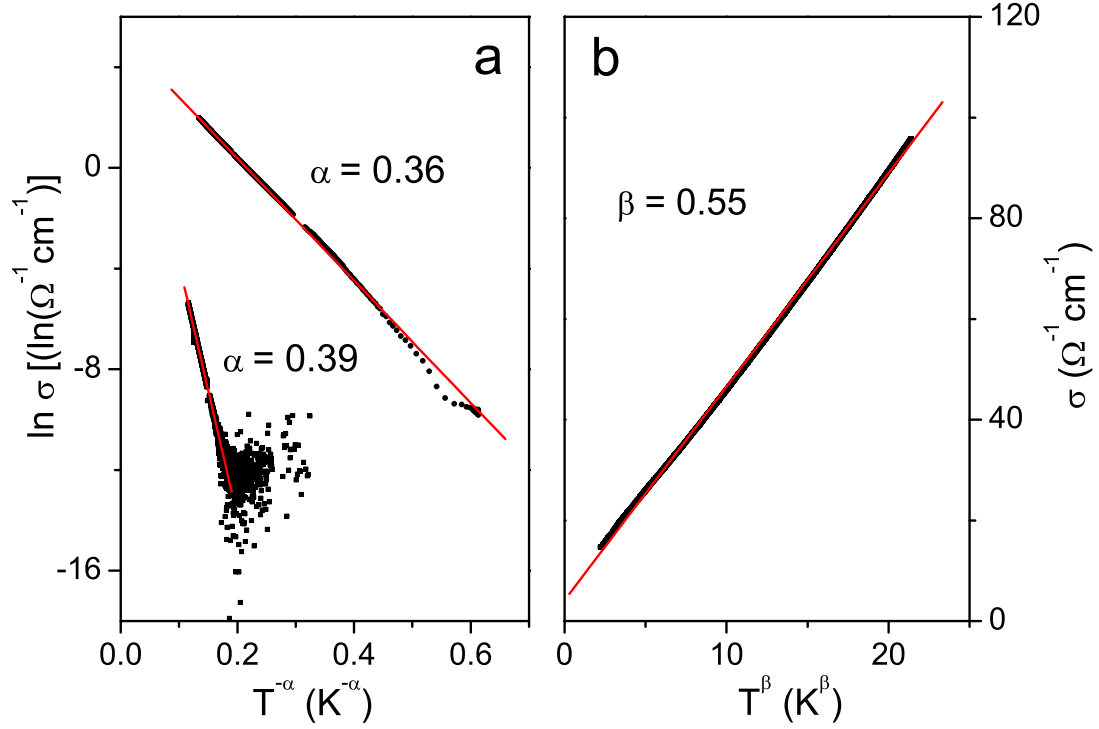


Figure 7: Temperature dependence of the electrical conductivity. Left figure: the temperature dependence for samples characterized by variable-range-hopping,  $\sigma \propto \exp(T_0/T)^\alpha$ . The exponents  $\alpha=0.39$  and  $\alpha=0.36$  are found for samples with W-content of 8.1 at% (sample #1) and 14.7 at% (sample #4), respectively. Right figure: temperature dependence for sample #8 with W-content of 31.8 at%. The conductivity increases with temperature as  $\sigma = \sigma_0 + aT^\beta$ , with  $\beta = 0.55$ ,  $\sigma_0=5.27 \Omega^{-1}\text{cm}^{-1}$  and  $a=4.08 \Omega^{-1}\text{cm}^{-1}\text{K}^{-1}$ .

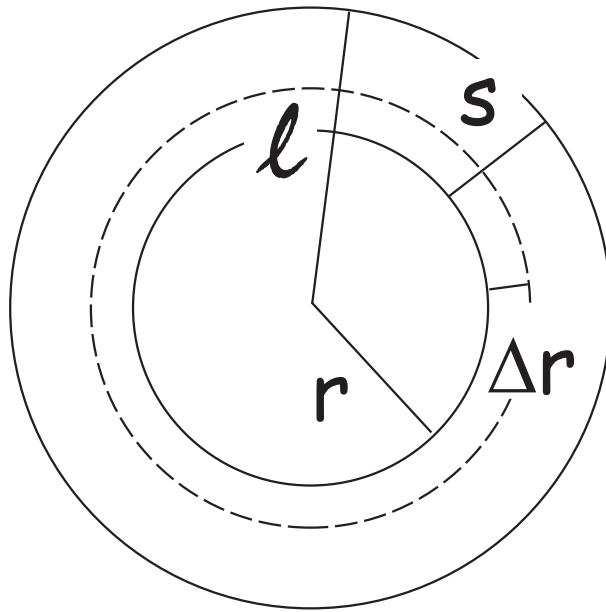


Figure 8: "Shell-model" used to model the time-dependent conductivity during the growth of a deposit. The model assumes that the metal W-particles have initially a radius  $r$ . The radius growth by  $\Delta r$  in the time  $\Delta t$  during the deposition, because of e-beam stimulated diffusion of W atoms.  $s$  is the separation between neighboring particles,  $l$  is the sum of  $s$  and  $r$ .



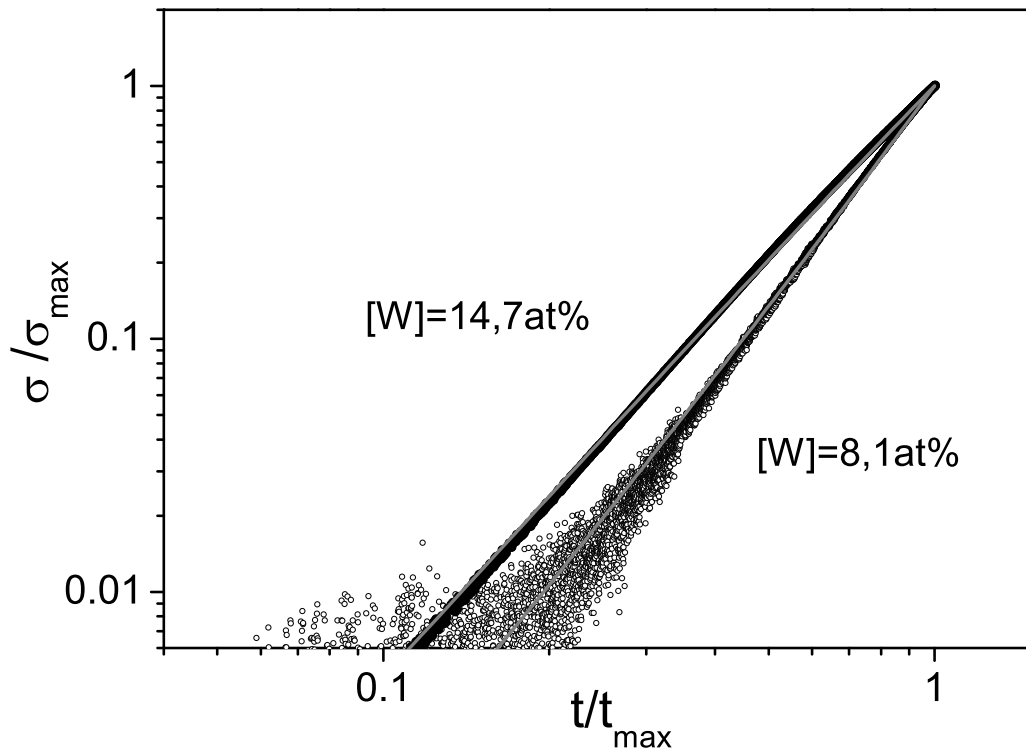


Figure 9: Conductivity vs. time during the growth process. The fit to the experimental data are made in the frame of the variable-range-hopping theory, see eq.( 1). The time dependence of the conductivity is implicit in the localization length  $\xi$  and in the effective activation energy  $W$ , according to the shell model of Fig. 8.

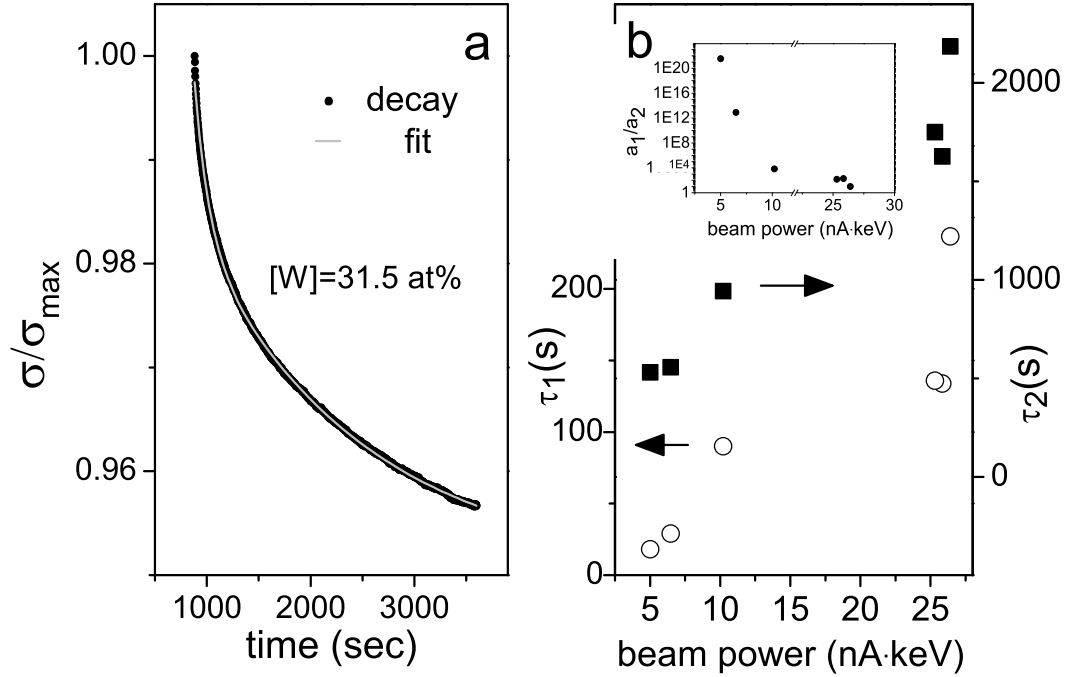


Figure 10: Decay of the conductivity during exposure to air. Left figure: the decay, as exemplary shown for sample #7, is described by the sum of two exponential decay channels according to  $\sigma = a_1 \exp(t/\tau_1) + a_2 \exp(t/\tau_2)$ . Each decay channel is associated to a tunneling mechanism: either between grains and trap sites in the matrix (decay constant  $\tau_1$ ) or between metal grains (decay constant  $\tau_2$ ). Right figure: value of the decay constants vs. beam power. The inset shows the ratio between the weight of the two tunneling mechanisms:  $a_1/a_2$ . For deposits prepared at small beam power the tunneling involving the matrix is dominant.